21nm x-ray laser Thomson scattering of laser-heated exploding foil plasmas

J. Dunn, B. Rus, T. Mocek, A. J. Nelson, M. E. Foord, W. Rozmus, H. A. Baldis, R. L. Shepherd, M. Kozlova, J. Polan, P. Homer, M. Stupka

April 30, 2008

21nm x-ray laser Thomson scattering of laser-heated exploding foil plasmas

J. Dunn [1], B. Rus [2], T. Mocek [2], A.J. Nelson [1], M.E. Foord [1], W. Rozmus [3], H.A. Baldis [4], R.L. Shepherd [1], M. Kozlová [2], J. Polan [2], P. Homer [2], and M. Stupka [2]

[1]*Lawrence Livermore National Laboratory, Livermore, CA 94551*
[2] *Institute of Physics / PALS Centre, 18221 Prague 8, Czech Republic*
[3] *University of Alberta, Edmonton, T6G 2J1, Canada*
[4] *Department of Applied Science, University of California, Davis, CA 95616, USA*

ABSTRACT

Recent experiments were carried out on the Prague Asterix Laser System (PALS) towards the demonstration of a soft x-ray laser Thomson scattering diagnostic for a laser-produced exploding foil. The Thomson probe utilized the Ne-like zinc x-ray laser which was double-passed to deliver ~1 mJ of focused energy at 21.2 nm wavelength and lasting ~100 ps. The plasma under study was heated single-sided using a Gaussian 300-ps pulse of 438-nm light (3ω of the PALS iodine laser) at laser irradiances of $10^{13} – 10^{14}$ W cm^{-2}. Electron densities of $10^{20} –10^{22}$ cm^{-3} and electron temperatures from 200 to 500 eV were probed at 0.5 or 1 ns after the peak of the heating pulse during the foil plasma expansion. A flat-field 1200 line mm^{-1} variable-spaced grating spectrometer with a cooled charge-coupled device readout viewed the plasma in the forward direction at 30° with respect to the x-ray laser probe. We show results from plasmas generated from ~1 μm thick targets of Al and polypropylene (C_3H_6). Numerical simulations of the Thomson scattering cross-sections will be presented. These simulations show electron peaks in addition to a narrow ion feature due to collective (incoherent) Thomson scattering. The electron features are shifted from the frequency of the scattered radiation approximately by the electron plasma frequency $\pm\omega_{pe}$ and scale as $n_e^{1/2}$.

Keywords: soft x-ray laser, laser-driven plasmas, Thomson scattering, exploding foil

1. INTRODUCTION

The understanding of highly ionized matter has required the development of new diagnostics and instrumentation to study the high temperature plasma conditions [1]. Optical techniques, later followed by the invention of the laser, allowed the probing of hot plasmas by means of visible light and ultraviolet (UV) interferometry [2] and Thomson scattering [3, 4]. In the latter case this rapidly evolved into robust diagnostic tools for probing plasmas from low electron density, $n_e \sim 10^{12} - 10^{14}$ cm^{-3}, magnetically confined plasmas [5, 6] to characterization of laser-produced plasmas at higher densities $n_e > 10^{19}$ cm^{-3}, for example [7, 8]. These have become routine diagnostics for determining quantitative measurements of plasma parameters including electron density, electron temperature, ion temperature and ion drift velocity n_e, T_e, T_i, and v_i, respectively. Typically, the measurements are made at $0.1\times n_c$, the critical density of the probe laser, which has limited the useful density, typically $10^{20} – 10^{21}$ cm^{-3}, that can be studied in laser–produced plasmas.

Recently, kilovolt x-ray energy probes have been developed to study high energy density plasmas [9, 10]. The main goal has been to extend the Thomson scattering technique to near-solid density plasma regimes. This has required the use of large laser facilities with multiple beams to generate the heated plasma as well as the significant keV x-ray fluence as the Thomson probe. Results were reported using the 30 kJ Omega laser facility [10] where 7 kJ of 351 nm laser light was used to generate a 4.75 keV probe to scatter from a radiatively driven beryllium plasma close to solid density. Soft x-ray lasers have potential as Thomson probes and have some advantages here. Their critical density is high enough to probe densities approaching 10^{24} cm^{-3} and so can access similar density regimes open to the keV x-rays. They are highly directional and so the laser energy can be transported effectively into the plasma of interest from meters away. The x-ray laser beam can be tightly focused onto a specific spatial region of the plasma by using an x-ray mirror: This allows spatial resolved probing in a uniformly heated region of a laser-produced plasma. Pulse duration can be in the range of a few

picoseconds [11, 12] to approximately 40 picoseconds [13] for different lasing schemes. This gives time-resolved scattering measurements defined by the x-ray laser pulse duration. A final advantage is that the line is extremely monochromatic without adjacent satellite lines that may be present to the long wavelength side of a He-α keV x-ray line. An initial study was conducted to look at the possibility of microjoule output picosecond x-ray laser to probe a 500 fs heated foil [14]. The objective was to study the feasability of using high resolution spectroscopy to study and spectrally resolve the Thomson scattering ion feature [14]. The conclusion was that the x-ray laser intensity had to be sufficiently high to overcome the bremsstrahlung continuum from thermal emission. Higher output above 100 µJ to 1 millijoule was useful for this type of experiment.

We will review a preliminary experiment conducted on the Prague Asterisk Laser System (PALS) where the 100 MW, millijoule Ne-like zinc $3p - 3s$ x-ray laser operating at 21.2 nm wavelength is available [15]. A simpler experiment is proposed [16] to use a more energetic probe beam to study a laser-heated exploding foil plasma and measure the forward-scattered electron features. This relaxes the very high spectral resolution requirement in [14] to detect the Thomson scattered peaks. Numerical simulations for the Thomson scattering cross-sections and the hydrodynamic simulations of the laser-heated exploding foil under study will be presented in the next section. The experiment will be described and results for two different laser-heated foil materials will be presented. The results will be discussed with prospects for future improvements.

2. THOMSON SCATTERING AND NUMERICAL SIMULATIONS

Figure 1(a) shows the basic experimental layout for the laser heated foil. The goal is to heat a ~1 µm thick foil from one side using the frequency-trebled PALS Iodine laser at 438 nm wavelength focused to a large spot size to achieve uniform density and temperature conditions. After a delay to allow the foil to blow down, the x-ray laser probe is incident from the left and focused in the center of the laser heated foil to sample the center of the heated conditions. The experimental target chamber layout in this case determined the observation geometry for the forward scattered direction at an angle θ from the incident beam. A spectrometer was used to spectrally resolve the Thomson scattered signal.
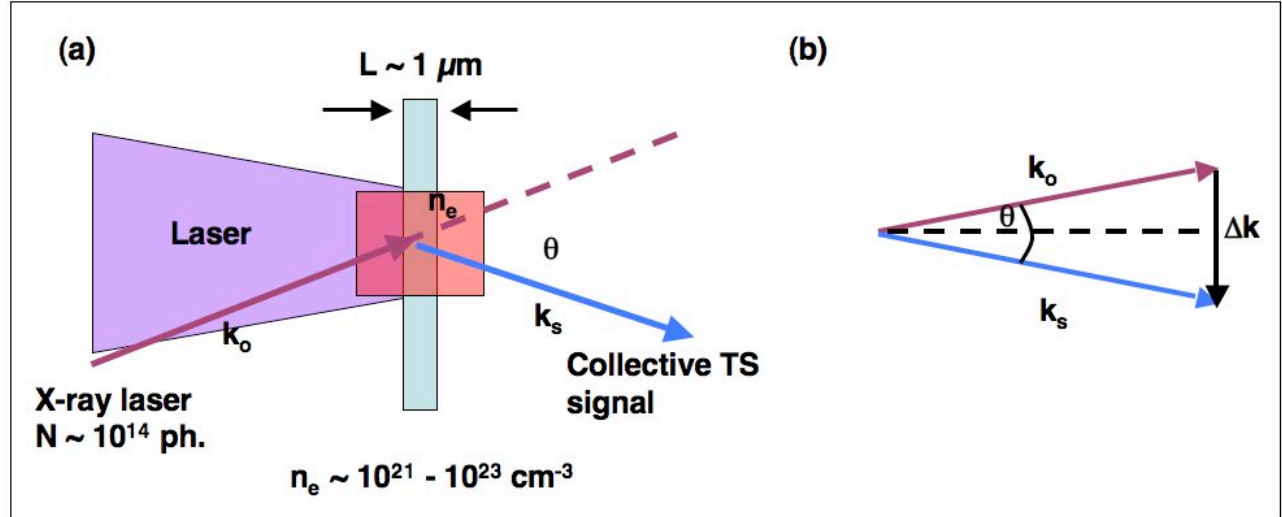

Figure 1: (a) Experimental setup showing laser-heated foil. X-ray laser probe, 1 mJ at 21.2 nm, is incident at time Δt when foil has blown down to desired electron density $n_e \sim 10^{21} - 10^{23}$ cm^{-3}. The Thomson scattered x-ray laser signal is measured by a spectrometer viewing at an angle θ. (b) Diagram showing wave vectors defining scattering geometry. The incident probe beam k_o, and scattered signal k_s, and differential scattering vector Δk are shown.

The Thomson scattered signal can be estimated for the expected plasma conditions of the experiment. The scattering cross-section, σ, is fairly low and can be written as $\sigma = \sigma_T S(\omega)$ [4, 5] where $\sigma_T = 8\pi r_o^2/3$ is the scattering cross-section of a single electron, r_o is the classical electron radius, and $S(\omega)$ is the spectral density function. The type of scattering whether incoherent non-collective (scattering on free electrons) or collective (scattering on plasma waves) is dependent on

the relation $\lambda_{XRL} < \lambda_D$ or $\lambda_{XRL} > \lambda_D$, respectively, where λ_{XRL} is the soft x-ray laser wavelength and λ_D is the Debye length [4, 5]. Kruer [17] writes $\lambda_D = (kT_e/4 \pi n_e e^2)^{1/2}$ and so scales as $743.4 \times (T_e(eV)/ n_e(cm^{-3}))^{1/2}$. For the expected experimental conditions as modeled below, $T_e \sim 400$ eV, $n_e \sim 10^{21}$ cm^{-3} , and $\lambda_{XRL} \sim 2.1 \times 10^{-6}$ cm, then the Debye length λ_D is $\sim 3.3 \times 10^{-7}$ cm. For higher density conditions the Debye length is always smaller and so incoherent collective scattering on the plasma waves is expected. The observed electron satellite features would be observed shifted $\pm \omega_{pe}$ from the central peak where ω_{pe} is the electron plasma frequency. Again from Kruer ω_{pe} is proportional to $(4 \pi n_e e^2/ m_e)^{1/2}$ and so scales as $5.64 \times 10^4 n_e(cm^{-3})^{1/2}$. Therefore the shift in the electron scattering feature is proportional to $n_e^{1/2}$. From Fig. 1(b) above, the differential scattering vector $\Delta k = 2 k_o \sin(\theta/2)$ and is used to determine the parameter α where $\alpha = 1/(\Delta k \lambda_D)$. The parameter α is dependent on the scattering angle, n_e, and T_e and defines the shape of the spectrum. For $\theta \sim 30°$ and $T_e \sim 400$ eV in the experiment, $\alpha \sim 1.4$ and 4.3 for $n_e \sim 10^{21}$ cm^{-3} and 10^{22} cm^{-3}, respectively. Figures 2(a) and (b) show Thomson scattering cross-sections in LTE plasmas with two values of electron density, $n_e=10^{21}$ cm^{-3} and $n_e=10^{22}$ cm^{-3}, at the electron temperature of 400 eV. The simulations, based on classical theory of Thomson scattering [4], show that in addition to the narrow central ion scattering feature the spectrum contains well-defined electron satellite peaks for a range of scattering angles θ. This figure illustrates some of the above discussion. The electron feature is well-defined in the forward scattered direction and can be measured with an instrument with moderate spectral resolution. The detected scattered signal is estimated to be $\sim 10^4$ photons when using a variable-spaced, flat-field grating spectrometer with a thermoelectrically cooled charge-coupled device (CCD) readout.
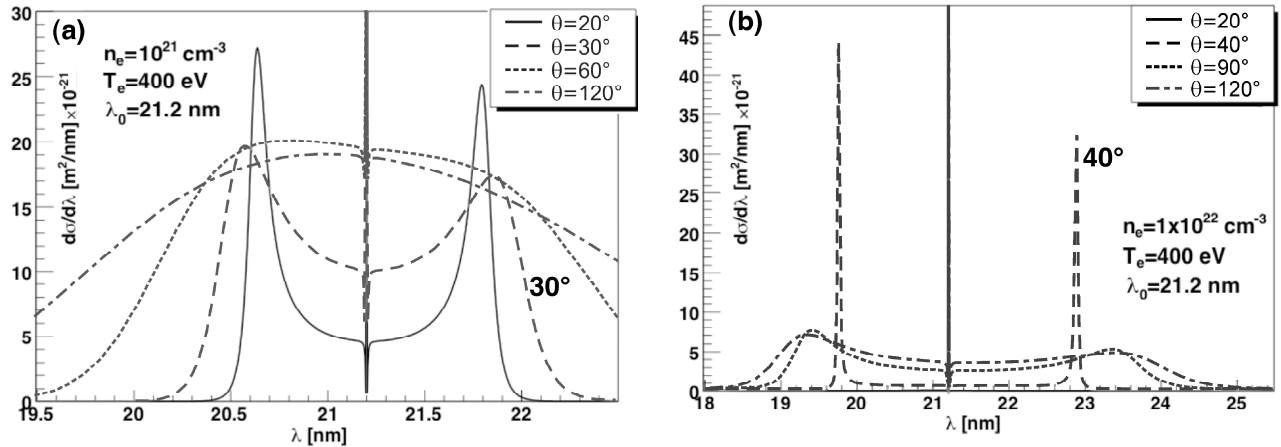

Figure 2: (a) Thomson scattering simulations for $\lambda = 21.2$ nm, $T_e \sim 400$ eV, $n_e \sim 10^{21}$ cm^{-3} at different scattering angles. Narrow spectral feature at 21.2 nm is ion scattering peak. (b) Thomson scattering simulations for $\lambda = 21.2$ nm, $T_e \sim 400$ eV, $n_e \sim 10^{22}$ cm^{-3} at different scattering angles.

Hydrodynamic simulations were performed for the laser-heated exploding foil target using the 1-D LASNEX code [18]. The 438 nm wavelength heating laser pulse was measured to be a Gaussian shape with 300 ps (FWHM) and was used as the input. Pure Lagrangian hydrodynamics were used. Laser ray-tracing and deposition packages were included with inverse bremsstrahlung as the main absorption mechanism. Radiation transport utilized flux limited multigroup diffusion with a flux limiter set at $f = 0.05$. The foils were zoned with 200 steps inside the target. Thermal conductivity and electron-ion coupling were from the Lee-More model [19] and the Quotidian Equation of State (QEOS) was used [20]. A 0.8μm aluminum foil and a 1.2 μm polypropylene (C_3H_6) foil targets, used in the experiments, were studied at laser irradiances of $10^{13} – 10^{14}$ W cm^{-2}. Figures 3(a) and (b) are plots showing electron temperature and density conditions versus position at different times relative to the peak of the laser pulse for the 10^{14} W cm^{-2} case on the 0.8 μm Al foil. The laser is incident from the left side and the initial foil position is at 0. It is worth noting that for all irradiances the laser pulse does not burnthrough the foils. As a result cold material is left at the back of the target, particularly in the low irradiance conditions. The laser ablation launches a cold flyer plate that extends several hundreds of microns drawing an extended plasma plume. This creates two distinct density zones that are quite uniform spatially but vary from $10^{20} – 10^{22}$ cm^{-3} for $0.5 – 1$ ns times after the peak of the pulse, Fig. 3(a). Maximum temperatures above 1 keV are achieved at the

peak of the heating pulse in the long scale length corona and rapid cooling occurs to $300 - 500$ eV within 1 ns, Fig. 3(b). More uniform density conditions are obtained with delays after the pulse has switched off as the foil blows down. There is a long scale length plasma that slowly drops in density with time but is relatively hot. The region at the back of the target is at higher density and gradually falls in time. However, the temperature of this region is relatively cold with large temperature gradients to the back of the foil, Fig. 3(b). This is confirmed in the experiments where the thermal emission lines from the laser-heated front of the foil are observed to be attenuated at the lower irradiances by the cold material at the back of the foil.
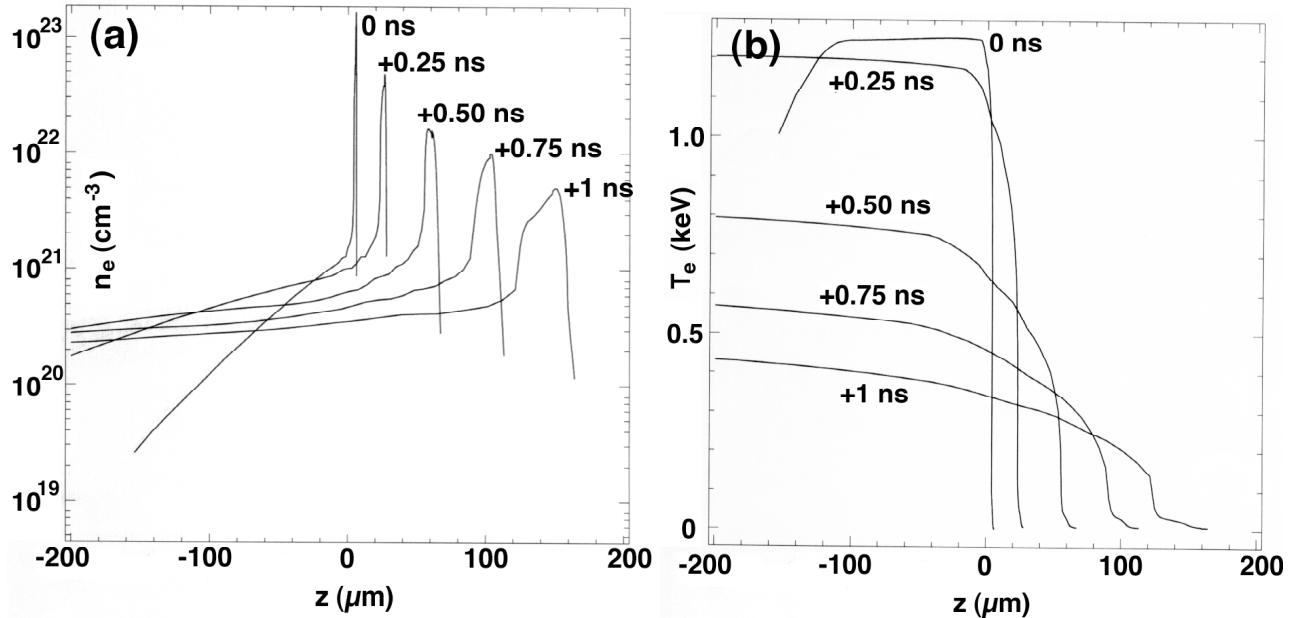

Figure 3: (a) LASNEX 1-D hydrodynamic simulations showing electron density versus spatial position for 0.8 μm aluminum foil irradiated at 10^{14} W cm^{-2} with a 300 ps (FWHM) 438 nm laser pulse. Laser is incident from the left and initial target position is at 0 μm. Times are relative to the peak of the laser pulse (t = 0 ns) and show density profile snapshot at potential Thomson probe times (t = 0, 0.25, 0.5, 0.75, 1 ns). (b) LASNEX 1-D hydrodynamic simulations showing electron temperature versus spatial position for 0.8 μm aluminum foil under similar laser conditions to (a).

3. EXPERIMENT DESCRIPTION

The experiment was conducted on the kilojoule-class 1.3 μm wavelength iodine laser of the Prague Asterix Laser System (PALS). This laser can deliver several synchronized beams at a repetition rate of 1 shot every 20 minutes. The Ne-like zinc 21.2 nm $3p - 3s$ laser line was generated by using up to 500 J in a Gaussian 300 ps (FWHM) laser pulse focused in a line onto a 3 cm long zinc slab target. A pre-pulse containing approximately $0.5 - 1\%$ of the total laser energy and delayed 10 ns before the main pulse was defocused and incident on the target [15]. The x-ray laser, generated by amplified spontaneous emission, was double-passed through the gain medium using a flat multilayer Mo:Si coated mirror with ~35% reflectivity. The x-ray laser beam, with $3 - 4$ mJ of output energy, was aligned and sent into the adjoining chamber, as shown in the experimental setup of Fig. 4. A retractable footprint monitor multilayer mirror was used to check the output and the pointing of the x-ray laser. The x-ray laser probe beam was focused onto the laser-heated foil target by using a multilayer coated off-axis parabola delivering 1 mJ soft x-ray energy on target. The important focusing and alignment of the 21 nm probe was achieved by looking at the the damage spot on a thin polymethyl methacrylate (PMMA) target and adjusting the target to parabola distance. The soft x-ray probe beam size was typically 20 μm (FWHM) on the target.

The foil heating beam was frequency trebled to 438 nm and contained up to 15 J of energy in 300 ps (FWHM). The heating beam could be delayed relative to the x-ray laser beam in order to change the arrival time of the x-ray laser for probing the plasma. The delays were typically 0 – 1 ns where the x-ray probe arrived after the heating beam relative to the peak of the laser pulse to probe various stages of foil plasma expansion. The heating beam focus was ~150 – 200 μm (FWHM) in diameter. A high magnification imaging system was used to overlap the two laser beams, the heating beam and the x-ray probe, by taking several shots where each beam was focused individually at low energy onto a 1.2 μm polypropylene foil. The damage burn spots were then studied and the two beams were carefully overlapped. The main diagnostic was a 1200 line mm^{-1} variable-spacing flat-field grating spectrometer with a thermoelectrically cooled, back-illuminated, charge-coupled device (CCD) 2048 × 512 (13.5 μm × 13.5 μm pixel) Andor DX440 camera. The spectrometer was set up to be operated without a slit by using the source size as a virtual slit. The initial alignment allowed the spectrometer to directly look at the x-ray laser beam by looking from behind the target and along the focusing axis of the parabola. A thick 4.5 μm aluminum foil was placed in front of the spectrometer to attenuate the signal. The 21.2 nm x-ray line was detected in the spectrum. The spectrometer was re-positioned as shown in Fig. 4 below, with a 0.8 μm Al light tight foil, to observe the Thomson scattering signal at 30°.
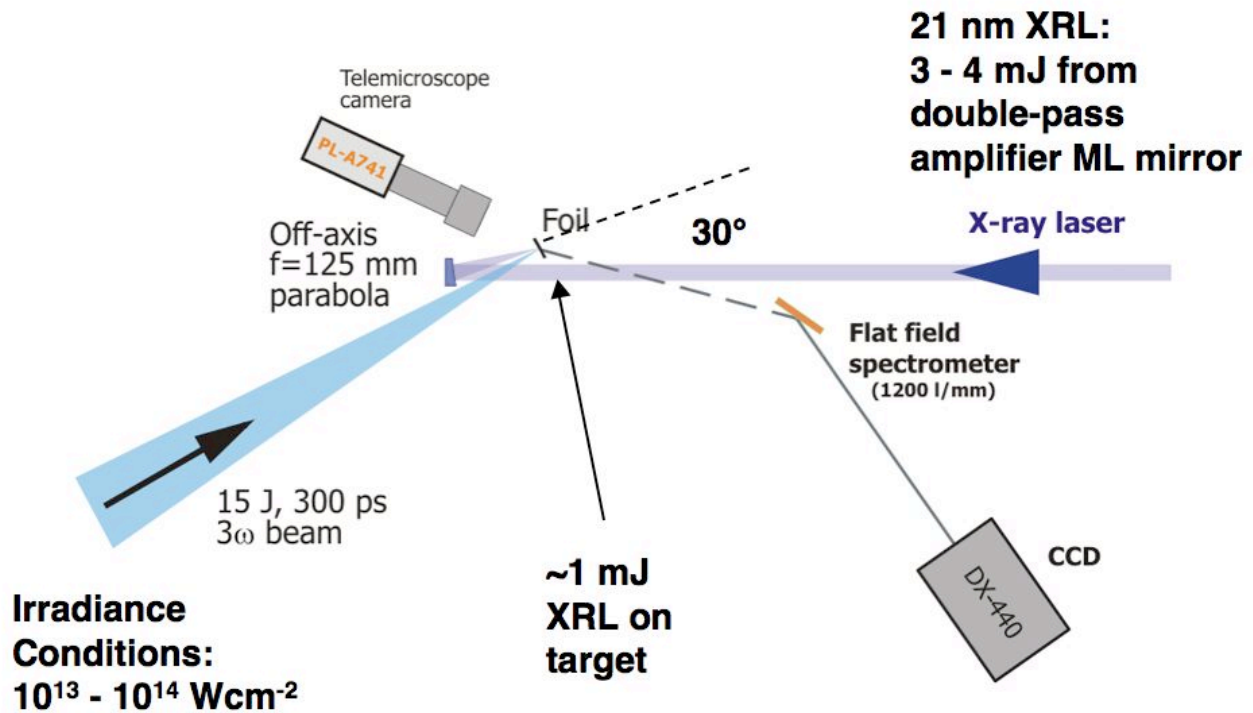

Figure 4: Experimental setup for soft x-ray Thomson scattering of laser-heated plasma. The x-ray laser is generated in adjoining chamber and focused into exploding foil using an off-axis parabola. Flat-field spectrometer observes Thomson scattered signal 30° in the forward direction.

4. RESULTS

Spectra were recorded on the 1200 line mm^{-1} flatfield spectrometer from the two foil targets for different irradiances and delays relative to the laser pulse. The spectral resolution was determined to be $\lambda/\Delta\lambda \sim 200$. Results are presented for the case of the highest laser irradiance of 10^{14} W cm^{-2}. The 0.8 μm aluminum foil was studied first and is shown in Fig. 5 (a). Intense thermal emission lines were observed across the full spectral region of interest. It should be noted that the x-ray laser lasts approximately 100 ps while the thermal lines will radiate over a substantially longer time of nanoseconds.

The main conclusion from the result below was that the weaker Thomson scattering signal would be difficult to detect among the forest of highly ionized aluminum emission lines. The choice of the time-integrated but higher dynamic range CCD detector, when compared to a streak camera, was justified to help in the detection of the scattered signal. Other interesting features were observed for the lower irradiance conditions on aluminum plasmas (not shown here). There appeared to be asymmetric lines and broad spectral bands that were thought to be due to the expansion of the plasma due to the cold flyer plate. This complicated the interpretation of the spectrum and is currently under detailed analysis.
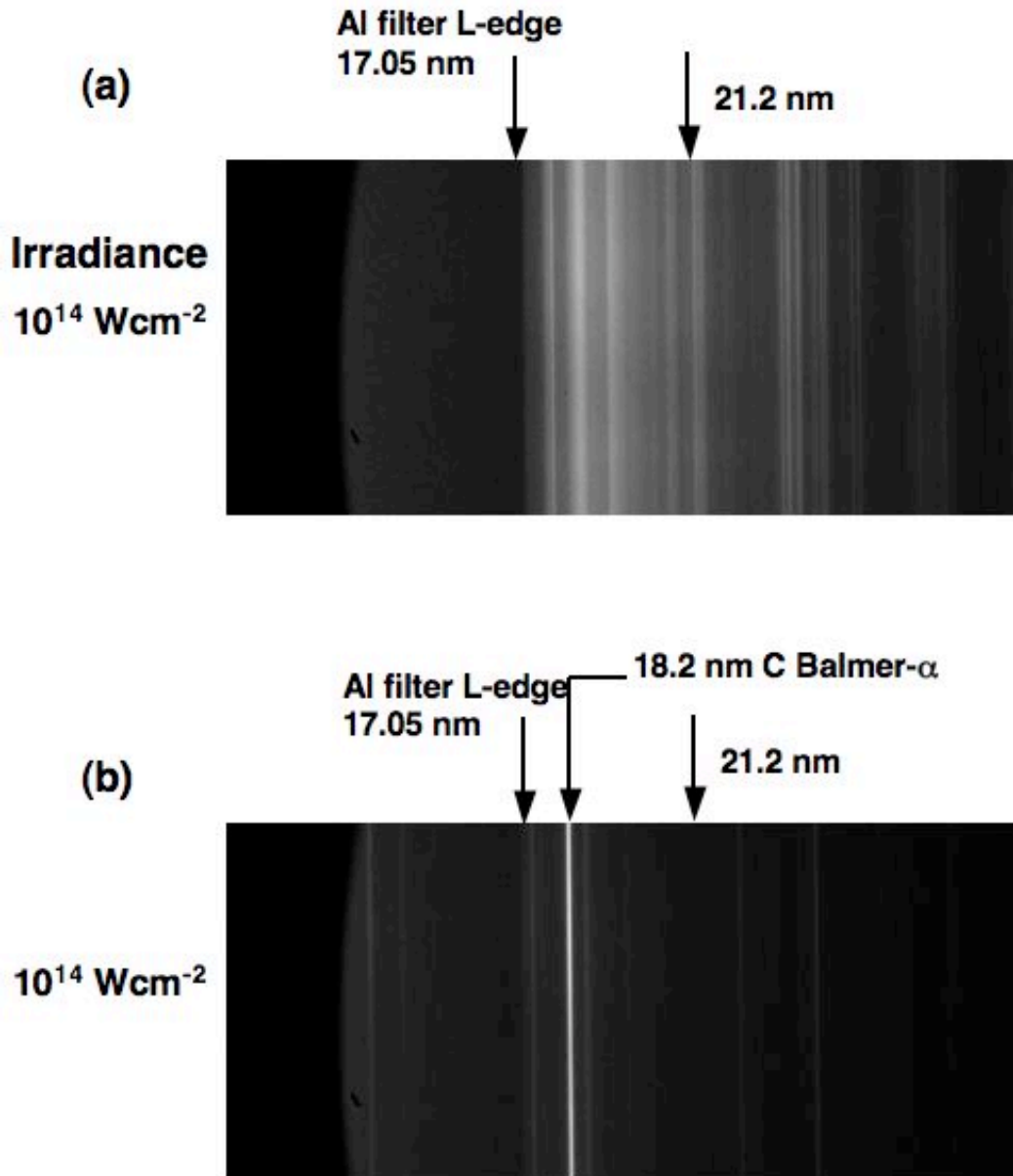

Figure 5: (a) Spectrum from 0.8 μm Al foil irradiated at 10^{14} W cm^{-2}. The aluminum L-edge at 17.05 nm from light tight spectrometer filter is labeled in both spectra. Spectral position of the 21.2 nm x-ray laser line is indicated. (b) Spectrum from 1.2 μm polypropylene foil irradiated under similar conditions. Fewer thermal emission lines are observed. The strong carbon Balmer-α line at 18.2 nm is labeled.

The 1.2 μm polypropylene target was found to be a better candidate plasma with fewer emission lines in the region of interest of a few nanometers either side of the 21 nm probe wavelength. The strongest thermal emission line in the spectrum was the hydrogen-like carbon Balmer-α line at 18.2 nm and is identified in Fig. 5(b). Again, at lower laser irradiances, asymmetric lines were observed to be present and all spectral features appeared to be attenuated by cold material at the back of the target. The carbon Balmer-α line and Balmer-β line at 13.59 nm were observed on all shots and were found to be spectrally narrow. This would support the idea that lower charge states of carbon may be emitted from the cooler extended plasma that was drawn by the flyer plate. A smooth bremsstrahlung continuum emission was the main feature in the region of interest with one or two extremely weak lines also present around 21 nm. These were observed with or without the x-ray laser probe. There was some indication of a possible enhancement of these weak features when the x-ray laser was fired [16]. The attenuation of the x-ray laser scattered signal by the cold material would be mitigated by two-sided laser heating and give a more uniform temperature plasma. This would also eliminate the flyer plate geometry. The most significant advance would be to carefully select the foil thickness to ensure burnthrough during the laser pulse.

5. DISCUSSION AND CONCLUSIONS

In summary, we have described a Thomson scattering experiment at soft x-ray wavelengths on a laser-produced plasma. Calculations were conducted for the spectral satellites of the electron scattering features and predicted conditions for incoherent collective scattering. Estimates of detected scattered photon number indicate a sizeable fraction of scattered photons that results in a low x-ray fluence and a fairly weak signal at the detector. Hydrodynamic plasma modeling and simulations of the Thomson scattered features for expected density and temperature conditions were presented. A preliminary experiment was performed using the PALS 21.2 nm x-ray laser. The overall geometry and setup was successfully tested in probing a laser-heated plasma with approximately 1 mJ of probe energy. Two exploding foils were studied at different laser irradiances. The 0.8 μm aluminum foil was found to contain many, strong thermal emission lines in the region of 21 nm. This made it unsuitable for detecting the weak Thomson scattered feature. In addition it was clear from the observations and the hydrodynamic simulations that the laser did not achieve foil burnthrough. Polypropylene was more suitable having a spectrally cleaner emission region at 21 nm with mainly bremsstrahlung continuum contribution. However, the presence of cold material at the back of the exploding foil results in significant absorption of the x-ray signal. The overall conclusion here is that the choice of foil material, thickness, laser plasma conditions, and irradiation geometry are important for optimizing the signal. Other improvements to be considered in the future include the use of a high-resolution, imaging spectrometer with collection optics to increase the signal. With sufficient signal the use of a time-resolved detector would discriminate against the long tail from the thermal emission.

ACKNOWLEDGMENTS

REFERENCES

1. R.H. Huddlestone and S.L. Leonard, editors, "Plasma Diagnostic Techniques", (Academic Press, NewYork London), pp. 627 (1965).
2. R.A. Alpher and D.R. White, "Interferometric measurement of electron concentrations in plasmas", *Phys. Fluids* **1**, 452 (1958).

3. G. Fiocco and E. Thompson, "Thomson scattering of optical radiation from an electron beam", *Phys. Rev. Lett.* **10**, 89 (1963).
4. E.E. Salpeter, "Electron density fluctuations in a plasma", *Phys. Rev.* **120**, 1528 (1960).
5. J. Sheffield, "Plasma Scattering of Electromagnetic Radiation" (Academic Press, New York) (1975).
6. D.E. Evans and J. Katzenstein, "Laser light scattering in laboratory plasmas", *Rep. Prog. Phys.* **32**, 207 (1969).
7. H.A. Baldis and C.J. Walsh, "Experimental Observations of Nonlinear Saturation of the Two-Plasmon Decay Instability", *Phys. Rev. Lett.* **47**, 1658 (1981).
8. B. La Fontaine, H.A. Baldis, D.M. Villeneuve, J. Dunn, G.D. Enright, J.C. Kieffer, H. Pépin, M.D> Rosen, D.L. Matthews, and S. Maxon, "Characterization of laser-produced plasmas by ultraviolet Thomson scattering", *Phys. Plasmas* **1**, 2329, (1994).
9. D. Riley, N.C. Woolsey, D. McSherry, I. Weaver, A. Djaoui, and E. Nardi, "X-Ray Diffraction from a Dense Plasma", *Phys. Rev. Lett.* **84**, 1704 (2000).
10. S.H. Glenzer, G. Gregori, R.W. Lee, F.J. Rogers, S.W. Pollaine, and O.L. Landen, "Demonstration of Spectrally Resolved X-Ray Scattering in Dense Plasmas", *Phys. Rev. Lett.* **90**, 175002 (2003).
11. A. Klisnick, J. Kuba, D. Ros, R. Smith, G. Jamelot, C. Chenais-Popovics, R. Keenan, S.J. Topping, C.L.S. Lewis, F. Strati, G.J. Tallents, D. Neely, R. Clarke, J. Collier, A.G. MacPhee, F. Bortolotto, "Demonstration of a 2-ps transient x-ray laser", P.V. Nickles, *Phys. Rev. A.* **65**, 033810 (2002).
12. J. Dunn, R.F. Smith, R. Shepherd, R. Booth, J. Nilsen, J.R. Hunter, and V.N. Shlyaptsev, "Temporal Characterization of a Picosecond Laser-Pumped X-ray Laser (for Applications)", *SPIE Int. Soc. Opt. Eng. Proc.* **5197**, 51-59 (2003).
13. J. Zhang, A.G. MacPhee, J. Nilsen, J. Lin, T.W. Barbee, Jr., C. Danson, M.H. Key, C.L.S. Lewis, D. Neely, R.M.N. O'Rourke, G.J. Pert, R. Smith, G.J. Tallents, J.S. Wark, and E. Wolfrum," Demonstration of Saturation in a Ni-like Ag X-Ray Laser at 14 nm", *Phys. Rev. Lett.* **78**(20), 3856 – 3860 (1997).
14. H.A. Baldis, J. Dunn, M.E. Foord, and W. Rozmus, "Thomson scattering diagnostic of solid density plasmas using x-ray lasers", *Rev. Sci. Instr.* **73**, 4223 (2002).
15. B. Rus, T. Mocek, A.R. Präg, M. Kozlová, G. Jamelot, A. Carillon, D. Ros, D. Joyeaux, and D. Phalippou, "Multimillijoule, highly coherent x-ray laser at 21 nm operating in deep saturation through double-pass amplification", *Phys. Rev. A* **66**, 063806 (2002).
16. B. Rus, J. Dunn, T. Mocek, A. J. Nelson, M. E. Foord, R. Shepherd, W. Rozmus, H. A. Baldis, M. Kozlová, J. Polan, P. Homer, and M. Stupka , "X-ray laser Thomson scattering at 21 nm of laser-heated high-density foil plasmas" in *X-ray Lasers 2006*, Proceedings of the 10th International Conference, August 20 – 25, 2006, Berlin, Germany, ed. P.V. Nickles and K.A. Janulewicz, Springer Proceedings in Physics **115**, 577 – 583 (2007).
17. W.L. Kruer, "The Physics of Laser Plasma Interactions", Publ. Addison-Wesley, pp182 (1987).
18. G.B. Zimmerman and W.L. Kruer, *Comments Plasma Phys. Control. Fusion* **2**, 51 - 61 (1975).
19. Y. T. Lee and R. M. More, *Phys. Fluids* **27**, 1273 (1984).
20. R. M. More, K. H. Warren, D. A. Young, and G. B. Zimmerman, *Phys. Fluids* **31**, 3059 (1988).